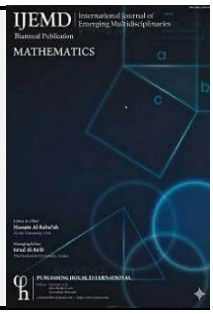
IJEMD-M, 4 (1) (2026) https://doi.org/10.54938/ijemd-m.2026.04.1.933

International Journal of Emerging Multidisciplinaries: Mathematics

Research Paper

Journal Homepage: www.ojs.ijemd.com

ISSN (print): 2790-1998



Unsteady Jeffrey Fluid Flow, Heat and Mass Transfer Along a Stretching Cylinder with Arrhenius Activation Energy

Muhammad Ali [*1] and Azeem Shahzad [1]

1. Department of Mathematical Sciences, University of Engineering and Technology (UET) Taxila, Pakistan

Abstract

In the present work, the unsteady flow, heat transfer and mass transfer of a Jeffrey fluid over a stretching cylinder has been formulated. There is a modified Arrhenius reaction in the concentration equation and the concentration reaction-heat contribution to the energy equation. The conservation laws are mapped to a coupled, 8th order boundary value problem which is integrated numerically with MATLAB code bvp4c and compared to 2 independent Newtonian benchmarks within 4×⟦10⟧^(-4). The next parameter sweep shows a clean separation of the parameters which influence the model, namely the skin-friction coefficient is only sensitive to the curvature, the unsteadiness and the two Jeffrey parameters, the momentum equation has no feedback on the thermal and concentration field, and the thermal and concentration field is sensitive to the other nine parameters. Of these, activation energy is the most influential, and is able to reduce the Sherwood number by nearly 25% of the range tested, whereas the Schmidt number is able to more than double the Sherwood number. The analysis reveals that the higher the curvature parameter and the Deborah number, the higher the rates of heat and mass transfer; however, the higher the ratio of relaxation-to-retardation time, the lower the rates of heat and mass transfer, and that this is a design parameter which a flat-plate treatment cannot offer.

Keywords: Jeffrey fluid; Stretching cylinder; Arrhenius activation energy.

[*] Corresponding author. Registration No. 2K24-MTH-MS-07.

Nomenclature

Symbol	Description
r, θ, z	Radial, azimuthal, and axial coordinates
$u,\ w$	Radial and axial velocity components; $v \equiv 0$ under axisymmetry
R	Cylinder radius
b	Constant characterizing the stretching rate
α_1	Parameter associated with temporal unsteadiness
t	Time variable
$T,\ C$	Local fluid temperature and species concentration
$T_w,\ C_w$	Temperature and concentration at the cylinder surface
$T_\infty,\ C_\infty$	Temperature and concentration of the ambient fluid
ρ	Fluid density
$\mu,\ \nu$	Dynamic viscosity and kinematic viscosity, respectively
λ	Ratio of relaxation time to retardation time
λ_1	Retardation time
$c_p,\ k$	Specific heat capacity and thermal conductivity, respectively
D_B	Species mass diffusivity
Q_0	Volumetric heat generation/absorption coefficient
$\Delta H,\ k_r$	Heat of reaction and chemical reaction-rate constant
$E_a,\ k_B$	Activation energy and Boltzmann constant
n	Exponent obtained from the fitted reaction-rate relation
η	Similarity coordinate
$f(\eta)$	Dimensionless stream function
$\theta(\eta)$	Dimensionless temperature function
$\phi(\eta)$	Dimensionless concentration function
K	Dimensionless curvature parameter
S	Dimensionless unsteadiness parameter
β	Deborah number
Pr	Prandtl number
Ec	Eckert number
Sc	Schmidt number
Q	Dimensionless heat generation/absorption parameter
Γ	Dimensionless Arrhenius reaction-strength parameter
δ	Dimensionless temperature-difference parameter
E	Dimensionless activation-energy parameter
σ	Dimensionless chemical reaction-rate parameter
C_f	Local skin-friction coefficient
$Nu_z,\ Sh_z$	Local Nusselt and Sherwood numbers
Re_z	Local Reynolds number

1 Introduction

The first to notice this was Sakiadis [1] who realised that when the wall itself is moving the boundary layer growing over it is modified, and the classical Blasius solution does not hold. This was later extended to a linearly stretching surface by Crane [2] to give a closed form solution which is now the standard check against any new stretching-flow analysis. The related problem of heat transfer was solved by Grubka and Bobba [3] and by Ali [4]. Wang [5] extended the flat sheet to a cylinder and considered the curvature parameter – K – that is used throughout the present work, while Ishak and Nazar [6] further investigated the parameter. A second extension by Ishak, Nazar, and Pop [7] enabled the stretching rate to fluctuate over time, and led to the introduction of the unsteadiness parameter S in this work.

All of these flat-plate and cylindrical studies make the Newtonian assumption, however, which is invalid for polymer melts, slurries, and many biological fluids which contain a trace of their deformation history. The Jeffrey model includes this memory with little added complexity, namely two additional parameters λ and β and is reduced to Newtonian exactly when both are zero, which is used for code verification in Section 4 later on. Prior studies have used it for sheets [8] or curved/stagnation-point surfaces [10, 11] but Hayat et al. [12] have studied mixed-convection Jeffrey flow over an inclined stretching cylinder with double stratification, the same geometry considered here but without chemical reaction.

There is also a parallel body of work that is based on reactions with an Arrhenius rate constant $k_r(T) = k_r^*(T/T_\infty)^n \exp\left(-E_a/(\kappa_B T)\right)$ that generates the activation-energy parameter E and the temperature-difference parameter δ along with the reaction-strength parameters, Γ and σ that will be introduced below. For the Jeffrey fluid, Samuel et al. [13] included the activation energy on a plane, uniform sheet. In the following papers, Jawad and co-workers [14, 15] put a Jeffrey fluid on a stretching cylinder, but in neither were there any chemical reactions.

The combination of a Jeffrey fluid, a stretching cylinder and a reaction that depends on the activation energy has therefore not been studied so far. The present study is based on Hayat et al. [12] inclined-cylinder configuration but is different in a sense that the double stratification effect is replaced by the Arrhenius reaction term while the unsteadiness, viscous dissipation and heat generation/absorption term are retained in the earlier model. The rest of the paper derives the governing equations and similarity reduction and numerically solves the resulting eighth-order boundary-value problem using `bvp4c`, against two independent Newtonian checks, and discusses a parametric study of the influence of curvature, unsteadiness, of the two Jeffrey parameters, and of the activation-energy parameters on the velocity, temperature, and concentration fields, relevant to processes like wire drawing and polymer extrusion, where the stretched surface is a cylinder rather than a sheet.

2 Mathematical Formulation

2.1 Physical Model

The flow of an unsteady Jeffrey fluid is assumed to be along an axisymmetric cylindrical surface with radius R which is assumed to be incompressible and stretching in the longitudinal direction throughout. The surface extends with velocity U_w (z,t)=bz/(1-α_1 t), where b is a fixed value, that determines the stretching rate, and the value of α_1 determines how such a rate varies with time: z is measured along the axis of the cylinder and the problem is formulated in cylindrical coordinates. The temperature and concentration off the wall is assumed to be the ambient temperature and concentration, T_∞ and C_∞, respectively, while the temperature and concentration on the wall is assumed to be constant, namely, T_w and C_w, respectively. With the assumption of axisymmetry, there is no swirl (v=0) and no dependence on θ ($\partial(\cdot)/\partial\theta=0$). The concentration field is overlaid with the field for a first order reaction rate constant with a modified Arrhenius reaction rate.

2.2 Governing Equations

The constitutive relation used here is that of the Jeffrey fluid, for which the Cauchy stress tensor superposes a retardation term onto the usual Newtonian (Navier–Stokes) stress: $\tilde{\tau} = -p\mathbf{I} + \frac{\mu}{1+\lambda}(\mathbf{A}_1 + \lambda_1 D\mathbf{A}_1/Dt)$, with $\mathbf{A}_1 = \text{grad}\mathbf{V} + (\text{grad}\mathbf{V})^t$ the first Rivlin–Ericksen tensor, λ the ratio of relaxation to retardation times, and λ_1 the retardation time; the ordinary Newtonian stress is recovered when $\lambda = \lambda_1 = 0$. Substituting this stress into the mass, momentum, energy, and species-concentration balances and invoking the usual boundary-layer (thin-shear-layer) simplification gives the following reduced system.

$$\frac{\partial u}{\partial r} + \frac{u}{r} + \frac{\partial w}{\partial z} = 0, \tag{1}$$

$$\rho\left(\frac{\partial w}{\partial t} + u\frac{\partial w}{\partial r} + w\frac{\partial w}{\partial z}\right) = \frac{\mu}{1+\lambda}\left[\frac{1}{r}\frac{\partial}{\partial r}\left(r\frac{\partial w}{\partial r}\right) + \lambda_1\frac{1}{r}\frac{\partial}{\partial r}\left(r\left[\frac{\partial^2 w}{\partial r\,\partial t} + u\frac{\partial^2 w}{\partial r^2} + w\frac{\partial^2 w}{\partial r\,\partial z}\right]\right)\right], \tag{2}$$

$$\rho c_p\left(\frac{\partial T}{\partial t} + u\frac{\partial T}{\partial r} + w\frac{\partial T}{\partial z}\right) = k\left(\frac{\partial^2 T}{\partial r^2} + \frac{1}{r}\frac{\partial T}{\partial r}\right) + \frac{\mu}{1+\lambda}\frac{\partial w}{\partial r}\left(\frac{\partial w}{\partial r} + \lambda_1\left[\frac{\partial^2 w}{\partial r\,\partial t} + u\frac{\partial^2 w}{\partial r^2} + w\frac{\partial^2 w}{\partial r\,\partial z}\right]\right) + Q_0(T - T_\infty) - \Delta H k_r^2\left(\frac{T}{T_\infty}\right)^n \exp\left(\frac{-E_a}{k_B T}\right)(C - C_\infty), \tag{3}$$

$$\frac{\partial C}{\partial t} + u\frac{\partial C}{\partial r} + w\frac{\partial C}{\partial z} = D_B\left(\frac{\partial^2 C}{\partial r^2} + \frac{1}{r}\frac{\partial C}{\partial r}\right) - k_r^2(C - C_\infty)\left(\frac{T}{T_\infty}\right)^n \exp\left(\frac{-E_a}{k_B T}\right). \tag{4}$$

The associated boundary conditions are

$$r = R: \quad w = \frac{bz}{1-\alpha_1 t}, \quad u = 0, \quad T = T_w, \quad C = C_w, \tag{5}$$

$$r \to \infty: \quad w \to 0, \quad T \to T_\infty, \quad C \to C_\infty. \tag{6}$$

2.3 Similarity Transformation

An axisymmetric stream function $\psi(r,z,t)$, defined through $u = -1/r\,\partial\psi/\partial z$ and $w = 1/r\,\partial\psi/\partial r$, satisfies the continuity equation (1) automatically. The stretching velocity motivates the following similarity variables: the curvature parameter $K = \sqrt{\nu(1-\alpha_1 t)/(bR^2)}$ (with $\nu = \mu/\rho$), the similarity coordinate $\eta = [(r^2 - R^2)/2R]\sqrt{b/[\nu(1-\alpha_1 t)]}$, the stream function $\psi = Rzr\sqrt{b\nu/(1-\alpha_1 t)}\,f(\eta)$, and the scaled temperature and concentration $\theta(\eta) = (T - T_\infty)/\Delta T$, $\phi(\eta) = (C - C_\infty)/\Delta C$, where $\Delta T = T_w - T_\infty$ and $\Delta C = C_w - C_\infty$. Introducing these into Eqs. (2) – (4)yields the closed, coupled, nonlinear ODE system

$$\begin{aligned}(f')^2 - ff'' + S\left(f' + \frac{\eta}{2}f''\right) - \frac{1}{1+\lambda}[(1+2K\eta)f''' + 2Kf''] \\ + \frac{\beta}{2(1+\lambda)}\{K\left[4\eta ff^{(4)} - 4\eta(f'')^2 + 6ff''' - 2f'f'' - 2S\eta^2 f^{(4)} - 10S\eta f''' - 6Sf''\right] \\ + \left[2ff^{(4)} - 2(f'')^2 - S\eta f^{(4)} - 4Sf'''\right]\} = 0,\end{aligned} \tag{7}$$

$$\begin{aligned}\left(\frac{S}{2}\eta - f\right)\theta' = \frac{1}{Pr}[(1+2K\eta)\theta'' + 2K\theta'] + Q\theta - \Gamma(1+\delta\theta)^n \exp\left(-\frac{E}{1+\delta\theta}\right)\phi \\ + \frac{Ec}{1+\lambda}(1+2K\eta)(f'')^2 + \frac{\beta Ec}{1+\lambda}(1+2K\eta)f''\left(\frac{3S}{2}f'' + \frac{S}{2}\eta f''' - ff''' + f'f''\right) \\ - \frac{K\beta Ec}{1+\lambda}f(f'')^2,\end{aligned} \tag{8}$$

$$\left(\frac{S}{2}\eta - f\right)\phi' = \frac{1}{Sc}[(1+2K\eta)\phi'' + 2K\phi'] - \sigma(1+\delta\theta)^n \exp\left(-\frac{E}{1+\delta\theta}\right)\phi, \tag{9}$$

subject to

$$f(0) = 0, \quad f'(0) = 1, \quad \theta(0) = 1, \quad \phi(0) = 1, \qquad f'(\infty) = 0, \quad \theta(\infty) = 0, \quad \phi(\infty) = 0. \tag{10}$$

The dimensionless parameters appearing in Eqs. (7)–(9) are defined in Table 1: K, S, β, λ, Pr, Ec, Q, δ, E, Γ, Sc, σ, n. The momentum equation is decoupled from the thermal and concentration fields, whereas the temperature and concentration equations remain coupled to the velocity solution through the convective terms; consequently, the nine purely thermal/concentration parameters (Pr, Ec, Q, Γ, δ, E, Sc, σ, n) shape heat and mass transfer without ever feeding back into the velocity field or the skin-friction coefficient.

Table 1: Dimensionless parameters governing Eqs. (9)–(9)

Parameter	Definition	Physical meaning
K	$\sqrt{\nu(1-\alpha_1 t)/(bR^2)}$	Curvature parameter; $K \to 0$ recovers the flat-plate limit
S	α_1/b	Unsteadiness parameter; $S = 0$ recovers the steady problem

Parameter	Definition	Physical meaning
β	$\lambda_1 b/(1-\alpha_1 t)$	Deborah number; strength of the Jeffrey memory (retardation) term
λ	–	Ratio of relaxation to retardation times; Newtonian limit requires $\lambda \to 0$ *and* $\beta \to 0$ together
Pr	$\nu\rho c_p/k$	Prandtl number
Ec	$b^2z^2/[c_p\Delta T(1-\alpha_1 t)^2]$	Eckert number (viscous dissipation)
Q	$Q_0(1-\alpha_1 t)/(\rho c_p b)$	Heat generation/absorption parameter
Γ	$\Delta H k_r^2 \Delta C(1-\alpha_1 t)/(\rho c_p \Delta T\, b)$	Arrhenius reaction-strength parameter (energy equation)
δ	$\Delta T/T_\infty$	Dimensionless temperature difference
E	$E_a/(k_B T_\infty)$	Dimensionless activation energy parameter
Sc	ν/D_B	Schmidt number
σ	$k_r^2(1-\alpha_1 t)/b$	Chemical reaction-rate parameter
n	–	Fitted-rate exponent of the modified Arrhenius law

2.4 Physical Quantities of Interest

The skin friction coefficient, local Nusselt number, and local Sherwood number reduce, in similarity form, to

$$\sqrt{Re_z}\,C_f = \frac{f''(0)}{1+\lambda}\left(1+\beta+\frac{3}{2}\beta S\right), \qquad Re_z^{-1/2}Nu_z = -\theta'(0), \qquad Re_z^{-1/2}Sh_z = -\phi'(0), \quad (11)$$

where $Re_z = U_w z/\nu$ is the local Reynolds number.

3 Numerical Methodology

The $f^{(4)}$ terms from the Jeffrey retardation term, along with the cylindrical curvature, make the momentum equation (7) fourth order, whilst the energy and concentration equations (8)–(9) are both second order. The full coupled system is therefore 8th order, matching the number of set boundary conditions (Eq. (10)). Each equation is rewritten in terms of its highest order and converted to a first order system in the state vector $\mathbf{y} = (f, f', f'', f''', \theta, \theta', \phi, \phi')$ on which bvp4c is applied to integrate with the residual-control collocation algorithm from Kierzenka and Shampine [16]. The far-field conditions are satisfied within the solver's tolerance and $f''(0)$, $\theta'(0)$, $\phi'(0)$ do not change much with further increases in $\eta_{\max}$ or mesh refinement, once the semi-infinite domain is cropped at a finite $\eta_{\max}$, in the range 8–10.

4 Validation of the Numerical Scheme

A numerical scheme is then tested against two Newtonian cases, ($\beta = \lambda = 0$) chosen together to cover all the equations in the model, since none of them have been combined with a Jeffrey fluid, an activation energy, and a stretching cylinder simultaneously.

Skin friction, curved case. In the absence of the curvature of the cylinder, with $\beta = \lambda = 0$ and $S = 0$ the momentum equation (7) reduces to $(1+2K\eta)f''' + 2Kf'' + ff'' - (f')^2 = 0$ – steady Newtonian flow over a

stretching cylinder with curved case curvature K. Fang et al. [17] have an exact similarity solution to the corresponding unsteady Navier–Stokes problem in terms of a Reynolds number $Re = ka_0^2/(2\nu)$; the similarity variable of Fang et al. is mapped onto the present one as follows: $r^2 = a_0^2\eta_{\text{Fang}} = R^2(1 + 2K\eta)$ with $K = 1/\sqrt{2Re}$, and $f''(0) = 2Kf''_{\text{Fang}}(1)$, which is confirmed independently by solving the reduced ODE directly.

Nusselt and Sherwood numbers, flat-plate case. If now $K = S = Q = \Gamma = Ec = \sigma = 0$ the energy and concentration equations can be reduced to $\theta'' + Pr\, f\theta' = 0$ and $\phi'' + Sc\, f\phi' = 0$ where the classical solution of Crane, $f(\eta) = 1 - e^{-\eta}$, is used. A single benchmark, Wang [18] covers these two, too: The same tabulated values of $-\theta'(0)$ against Pr work equally as well when Pr is replaced by the Sherwood number Sc.

Table 2: Comparison of the present results with benchmark studies in two Newtonian ($\beta = \lambda = 0$) limiting cases

Quantity	Parameter	Benchmark	Present	Diff.
Skin friction $f''(0)$, curved case ($S = 0$), vs. Fang et al. **[Error! Reference source not found.]**				
$f''(0)$	$K = 0.7071$ ($Re = 0.5$)	-1.2476	-1.2477	7×10^{-5}
$f''(0)$	$K = 0.5000$ ($Re = 1$)	-1.1778	-1.1778	3×10^{-5}
$f''(0)$	$K = 0.3536$ ($Re = 2$)	-1.1271	-1.1271	1×10^{-5}
$f''(0)$	$K = 0.2236$ ($Re = 5$)	-1.0811	-1.0811	2×10^{-6}
$f''(0)$	$K = 0.1581$ ($Re = 10$)	-1.0576	-1.0576	1×10^{-6}
Nusselt number $-\theta'(0)$, flat-plate case ($K = S = 0$), vs. Wang **[Error! Reference source not found.]**				
$-\theta'(0)$	$Pr = 0.07$	0.0656	0.065564	3.6×10^{-5}
$-\theta'(0)$	$Pr = 0.2$	0.1691	0.169089	1.1×10^{-5}
$-\theta'(0)$	$Pr = 0.7$	0.4539	0.453916	1.6×10^{-5}
$-\theta'(0)$	$Pr = 2$	0.9114	0.911358	4.2×10^{-5}
$-\theta'(0)$	$Pr = 7$	1.8954	1.895404	4.1×10^{-6}
$-\theta'(0)$	$Pr = 20$	3.3539	3.353917	1.7×10^{-5}
$-\theta'(0)$	$Pr = 70$	6.4622	6.462519	3.2×10^{-4}
Sherwood number $-\phi'(0)$, flat-plate case ($K = S = 0$), vs. Wang [18] with Sc for Pr				
$-\phi'(0)$	$Sc = 0.07$	0.0656	0.065564	3.6×10^{-5}
$-\phi'(0)$	$Sc = 0.2$	0.1691	0.169089	1.1×10^{-5}
$-\phi'(0)$	$Sc = 0.7$	0.4539	0.453916	1.6×10^{-5}
$-\phi'(0)$	$Sc = 2$	0.9114	0.911358	4.2×10^{-5}
$-\phi'(0)$	$Sc = 7$	1.8954	1.895404	4.1×10^{-6}
$-\phi'(0)$	$Sc = 20$	3.3539	3.353917	1.7×10^{-5}
$-\phi'(0)$	$Sc = 70$	6.4622	6.462519	3.2×10^{-4}

The energy and concentration equations are identical at $K = S = Q = \Gamma = Ec = \sigma = 0$ – that is, at the Sherwood-number rows in table 2, the Nusselt-number rows reproduce themselves, but only because the equations are identical, not because of a coincidence of the solver. All the entries of the table are within a tolerance of 4×10^{-4}, and within a tolerance of 10^{-4}, everywhere except for the largest-Pr/Sc line which is used in the above similarity reduction, in the first-order recasting in Section 3 and in the `bvp4c` settings used here, and is continued in the unchanged form into the parametric study of Section 5.

5 Results and Discussion

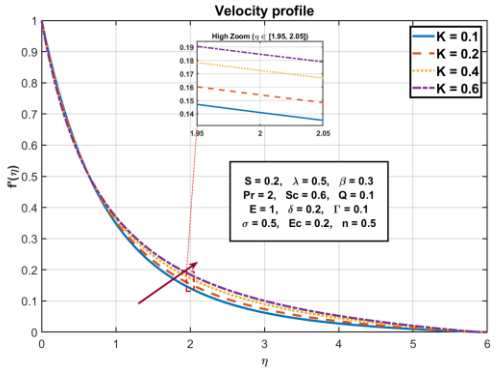
Table 3: Physical skin friction coefficient $C_f^* = \frac{1}{1+\lambda}\left(1+\beta+\frac{3}{2}\beta S\right) f''(0)$ (where $f''(0)$ is computed and reported in the table), local Nusselt number $Re_z^{-1/2} Nu_z = -\theta'(0)$, local Sherwood number $Re_z^{-1/2} Sh_z = -\phi'(0)$

Param.	Value	$f''(0)$	$-\theta'(0)$	$-\phi'(0)$
K	0.1	−1.060659	0.562969	0.563002
	0.2	−1.096178	0.576578	0.615605
	0.4	−1.166057	0.627991	0.716681
	0.6	−1.234589	0.691627	0.813496
S	0.1	−1.046340	0.664368	0.632731
	0.15	−1.071254	0.622528	0.624153
	0.2	−1.096178	0.576578	0.615605
	0.3	−1.146026	0.468527	0.598722
β	0.1	−0.985427	0.550959	0.607423
	0.3	−1.096178	0.576578	0.615605
	0.5	−1.198151	0.593478	0.622398
	0.7	−1.293393	0.604640	0.628158
λ	0.1	−1.295868	0.600083	0.627689
	0.5	−1.096178	0.576578	0.615605
	1	−0.940498	0.541680	0.604277
	1.5	−0.836011	0.506423	0.595570
Pr	1	−1.096178	0.411824	0.618777
	2	−1.096178	0.576578	0.615605
	3	−1.096178	0.762400	0.612804
	4	−1.096178	0.929758	0.610736
Ec	0.1	−1.096178	0.673664	0.615071
	0.2	−1.096178	0.576578	0.615605
	0.3	−1.096178	0.479491	0.616138
	0.4	−1.096178	0.382404	0.616670
Q	0	−1.096178	0.753172	0.614033
	0.05	−1.096178	0.671550	0.614731
	0.1	−1.096178	0.576578	0.615605
	0.2	−1.096178	0.309300	0.618399
δ	0.1	−1.096178	0.570335	0.606534
	0.2	−1.096178	0.576578	0.615605
	0.3	−1.096178	0.582651	0.624431
	0.4	−1.096178	0.588556	0.633013
E	1	−1.096178	0.576578	0.615605
	2	−1.096178	0.514755	0.535812
	3	−1.096178	0.486900	0.500069
	4	−1.096178	0.475090	0.484861
Γ	0.1	−1.096178	0.576578	0.615605
	0.2	−1.096178	0.684596	0.614497
	0.3	−1.096178	0.790936	0.613404
	0.4	−1.096178	0.895629	0.612326
Sc	0.2	−1.096178	0.602224	0.429081
	0.6	−1.096178	0.576578	0.615605

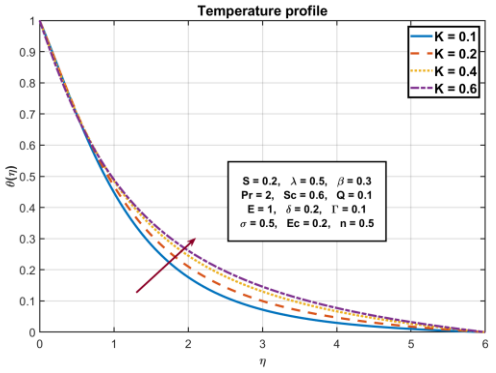
Param.	Value	$f''(0)$	$-\theta'(0)$	$-\phi'(0)$
	1	−1.096178	0.558039	0.781049
	1.4	−1.096178	0.544523	0.929052
σ	0.2	−1.096178	0.584956	0.534369
	0.5	−1.096178	0.576578	0.615605
	0.8	−1.096178	0.569638	0.688260
	1.1	−1.096178	0.563786	0.754254
n	0	−1.096178	0.571952	0.608860
	0.5	−1.096178	0.576578	0.615605
	1	−1.096178	0.581470	0.622755
	1.5	−1.096178	0.586644	0.630336

Only the skin friction, K, S, β and λ (which are part of the momentum equation (7)) are the parameters that change the value of $f''(0)$. All nine of the remaining parameters, Pr, Ec, Q, Γ, δ, E, Sc, σ and n only appear in the energy and/or concentration equations. The one-way coupling noted above should be remembered throughout this section as it will be treated sequentially for each group of parameters.

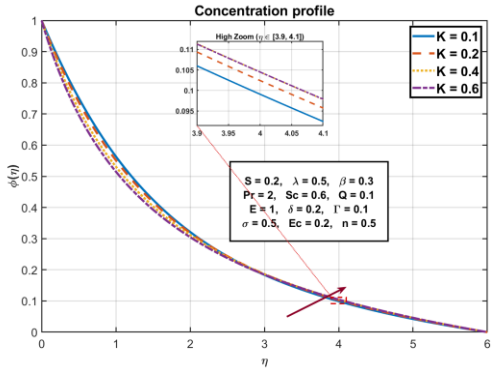
5.1 Momentum-Coupled Parameters: Curvature (K), Unsteadiness (S), Deborah Number (β), and Relaxation–Retardation Ratio (λ)



(a) $f'(\eta)$



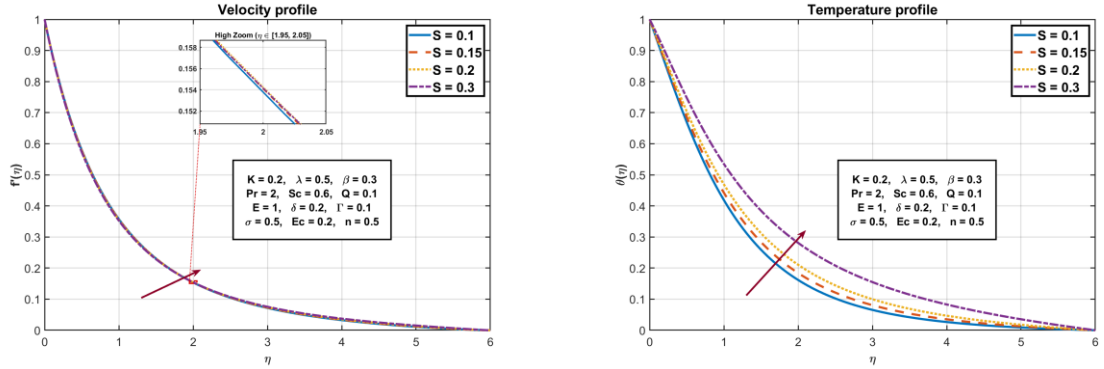
(b) $\theta(\eta)$



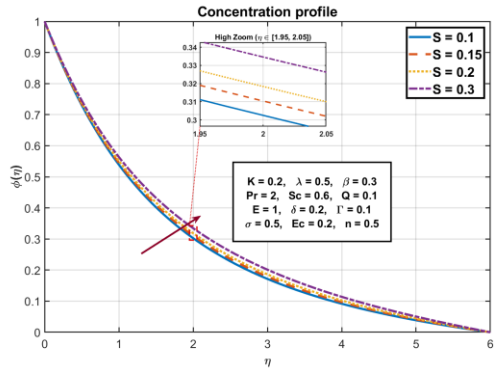
(c) $\phi(\eta)$

Figure 1: $f'(\eta)$

Figure 1 shows the effect of the curvature parameter K on velocity, temperature and concentration profiles. The larger K is, the better the velocity profile is throughout the boundary layer. The thermal field is also stronger with higher curvature, as seen in the temperature profile. However, the concentration profile has a non-uniform response: it drops off near the wall, then has a crossover further away from the cylindrical surface. These profile variations are not all identical for all the fields, but for K increased the wall gradients grow which results in an increase of the skin friction coefficient, the local Nusselt number, and the local Sherwood number, as indicated in Table 3: $\sqrt{Re_z}\,C_f$ decreases from -1.0607 to -1.2346; $Re_z^{-1/2}Nu_z$ increases from 0.5630 to 0.6916; and $Re_z^{-1/2}Sh_z$ increases even more from 0.5630 to 0.8135.



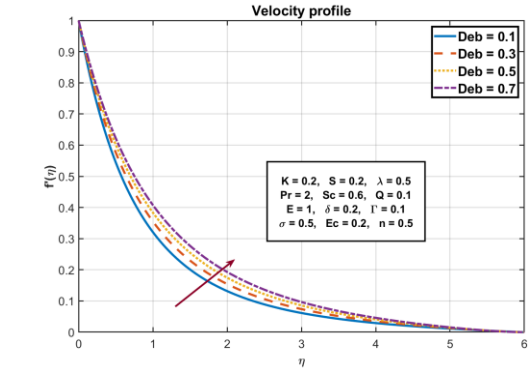
(a) $f'(\eta)$ **(b)** $\theta(\eta)$



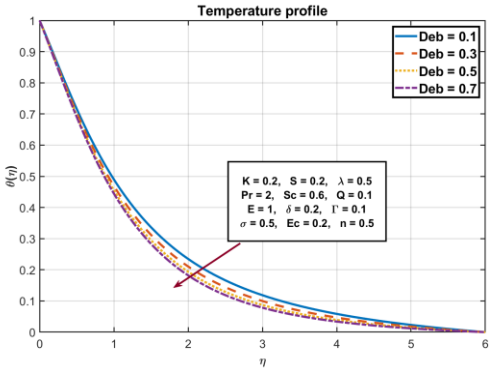
(c) $\phi(\eta)$

Figure 2: $f'(\eta)$

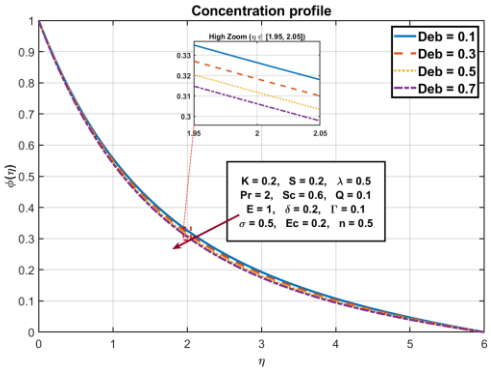
The unsteadiness parameter differs in behaviour (Fig. 2). While the velocity gradient of the wall is increased as S increases from 0.1 to 0.3 the response of the thermal and concentration fields is opposite; less time is available for the thermal and concentration fields to develop before being convected downstream, so both of these fields grow as S increases, with the decrease in $Re_z^{-1/2}Nu_z$ from 0.6644 to 0.4685 and a decrease in $Re_z^{-1/2}Sh_z$ from 0.6327 to 0.5987 being less steep. As predicted, the steady stretching-cylinder limit is recovered when $S = 0$.



(a) $f'(\eta)$



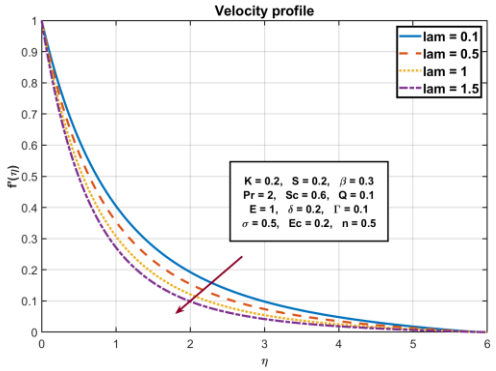
(b) $\theta(\eta)$



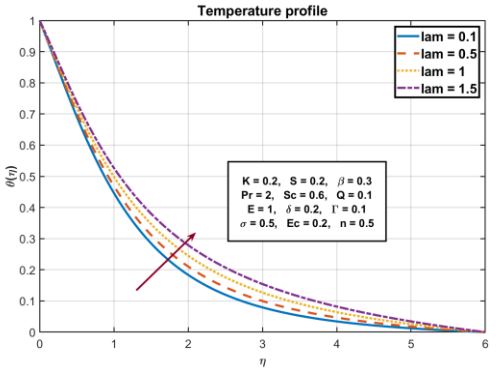
(c) $\phi(\eta)$

Figure 3: $f'(\eta)$

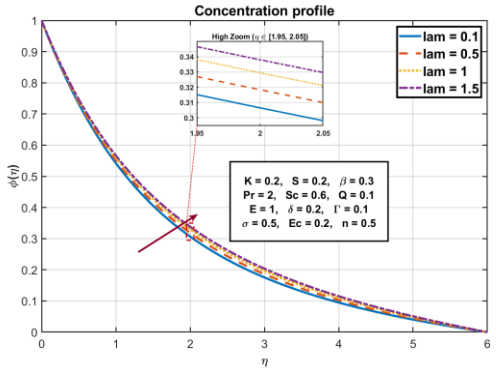
The Deborah number has a similar qualitative effect on the momentum field as curvature does on the momentum field (Fig. 3), by amplifying the elastic contribution to the stress. β does not explicitly appear in the energy and concentration equations, but it appears in Eqs. (8)–(9) through the convective terms, making the elastic contribution to the stress increase as β increases from 0.1 to 0.7 (from $Re_z^{-1/2}Nu_z = -0.9854$ to $Re_z^{-1/2}Nu_z = -1.2934$ and from $Re_z^{-1/2}Sh_z = 0.6074$ to $Re_z^{-1/2}Sh_z = 0.6282$). That is, the higher β the greater the heat- and mass-transfer rates at the wall, just because the boundary layers through which θ and ϕ must decrease from wall value to zero are thinned.



(a) $f'(\eta)$



(b) $\theta(\eta)$

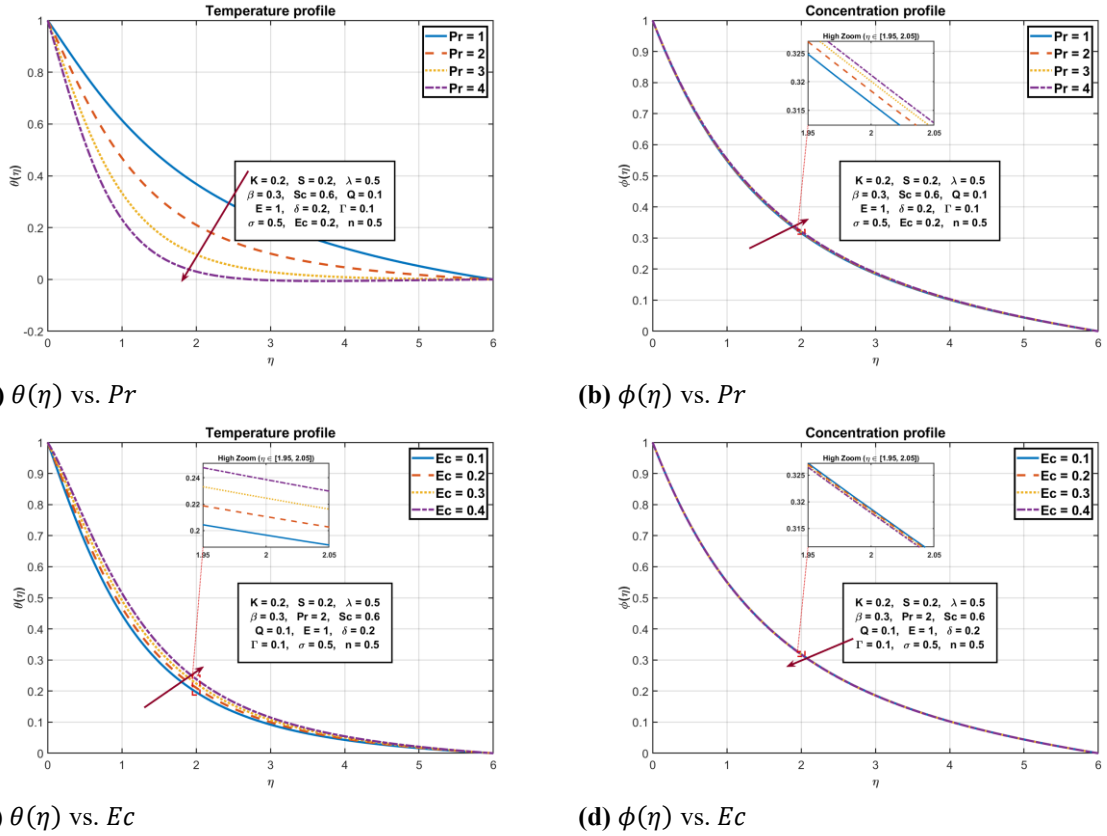


(c) $\phi(\eta)$

Figure 4: $f'(\eta)$

If one increases the retardation time, λ, from 0.1 to 1.5 (Fig. 4), the elastic response will be damped more and more, even when the relaxation time is fixed at $\beta \neq 0$ and $= 0.1$. Consequently $\sqrt{Re_z}\, C_f$ shrinks in magnitude from -1.2959 to -0.8360, while $Re_z^{-1/2} Nu_z$ and $Re_z^{-1/2} Sh_z$ ease down slightly, from 0.6001 to 0.5064 and from 0.6277 to 0.5956, respectively. The Newtonian limit is obtained as $\beta \to 0$ and $\lambda \to 0$ together; the flat-plate limit occurs as $K \to 0$ but λ does not necessarily go to 0.

5.2 Thermal Parameters: Prandtl (Pr) and Eckert (Ec) Numbers



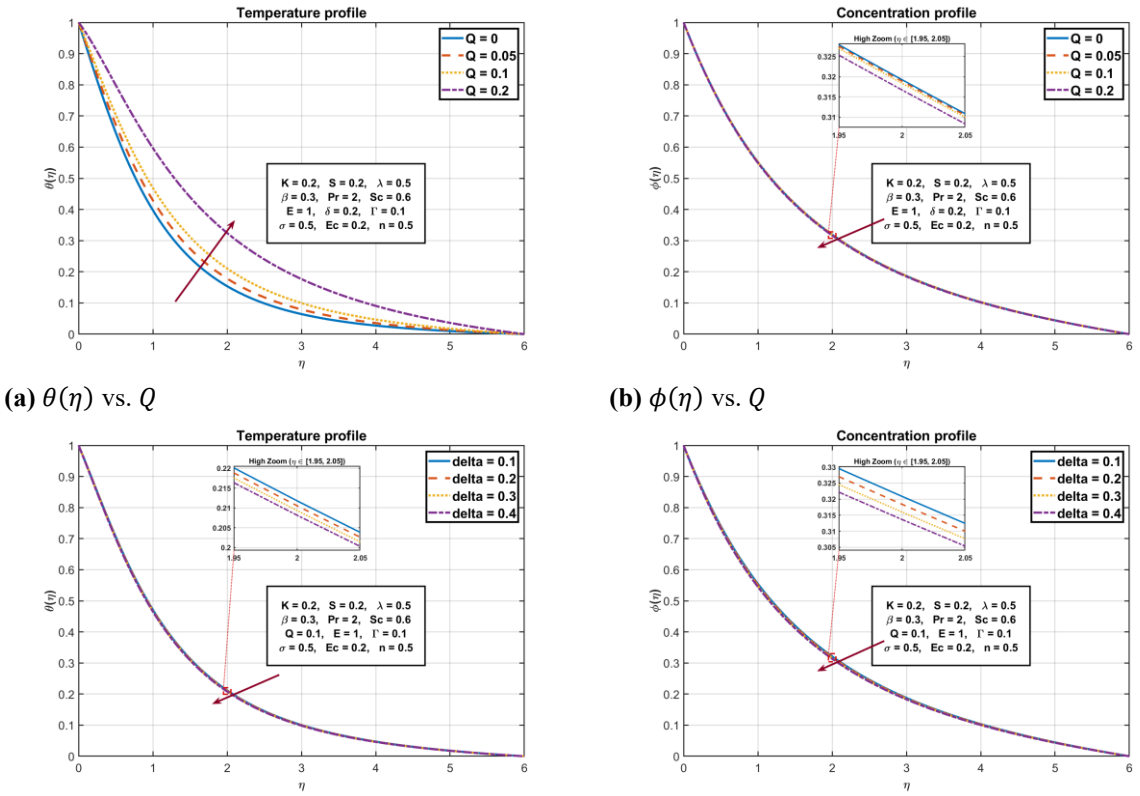
(a) $\theta(\eta)$ vs. Pr **(b)** $\phi(\eta)$ vs. Pr

(c) $\theta(\eta)$ vs. Ec **(d)** $\phi(\eta)$ vs. Ec

Figure 5: $\theta(\eta)$ vs. Pr

As seen directly from Table 3 the values of $f'(\eta)$ and $f''(0)$ are independent of Pr when it is varied. Its role instead is to reduce the thermal diffusivity compared to the momentum diffusivity, such that as Pr is increased from 1 to 4: $Re_z^{-1/2}Nu_z$ increases more than twice (from 0.4118 to 0.9298), while $Re_z^{-1/2}Sh_z$ changes very slightly (from 0.6188 to 0.6107). The Eckert number is different, however: If Ec is raised from 0.1 to 0.4 more viscous dissipation, both from the Newtonian and Jeffrey parts, raises the temperature of the fluid in the boundary layer. Since $\theta(0) = 1$ is fixed at the wall, this warming flattens the temperature gradient there, so $Re_z^{-1/2}Nu_z$ drops from 0.6737 to 0.3824 – nearly by half – while $Re_z^{-1/2}Sh_z$ is essentially unaffected ($0.6151 \rightarrow 0.6167$).

5.3 Heat Generation (Q) and Temperature-Difference (δ) Parameters



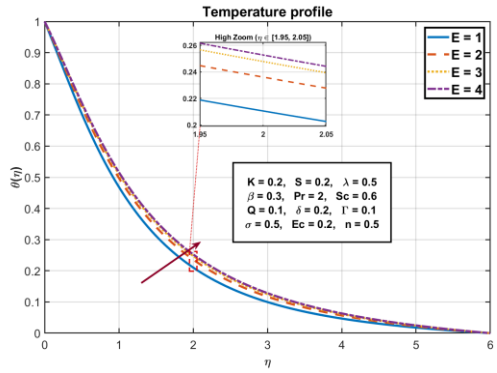
(a) $\theta(\eta)$ vs. Q **(b)** $\phi(\eta)$ vs. Q

(c) $\theta(\eta)$ vs. δ **(d)** $\phi(\eta)$ vs. δ

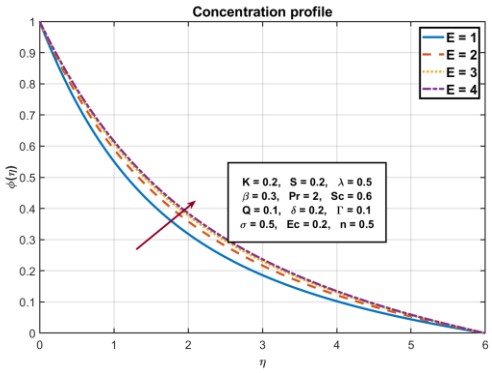
Figure 6: $\theta(\eta)$ vs. Q

The parameter Q has the greatest effect on the Nusselt number, $Re_z^{-1/2}Nu_z$ changing by more than half when Q changes from 0 to 0.2 ($Q > 0$ corresponds to the case of internal heat generation which warms the fluid and flattens the wall temperature gradient; $Q < 0$ would act in the opposite sense). $Re_z^{-1/2}Sh_z$ is only slightly affected, changing by less than 0.05 when Q changes from 0 to 0.2. The influence of the temperature-difference parameter δ is more modest since it enters through the modified Arrhenius factor $(1 + \delta\theta)^n \exp[-E/(1 + \delta\theta)]$ linking Eqs. (8) and (9) and this increases slightly the $Re_z^{-1/2}Nu_z$ and $Re_z^{-1/2}Sh_z$ from 0.5703 to 0.5886 and from 0.6065 to 0.6330 respectively for increasing δ from 0.1 to 0.4..

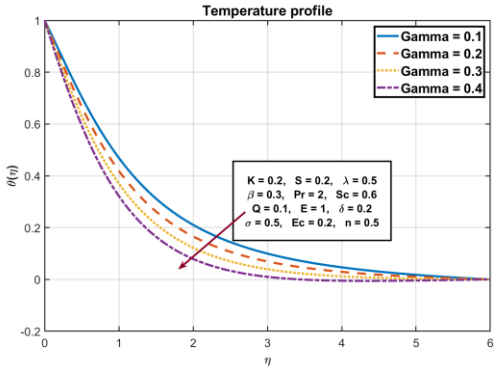
5.4 Activation Energy (E) and Reaction-Strength (Γ) Parameters



(a) $\theta(\eta)$ vs. E



(b) $\phi(\eta)$ vs. E

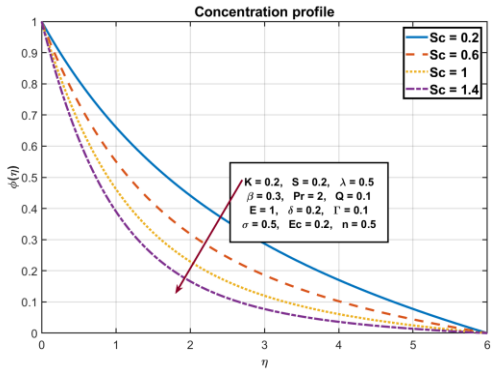


(c) $\theta(\eta)$ vs. Γ

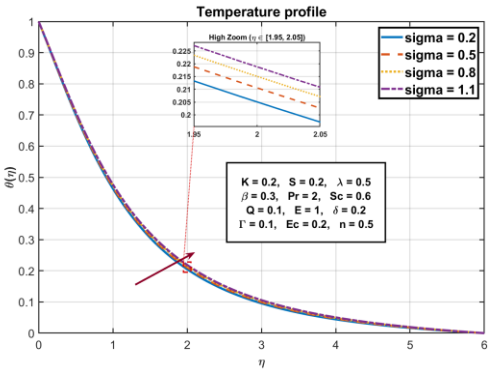
Figure 7: $\theta(\eta)$ vs. E

This is where that the activation-energy physics is most apparent. The larger the value of E the quicker the Arrhenius exponential decays, the slower the reaction, and the more species will be consumed as $\phi(\eta)$ accumulates through the boundary layer from 1 to 4. The concentration boundary layer thickens proportionately and the $Re_z^{-1/2}Sh_z$ decreases dramatically from 0.6156 to 0.4849 – almost a 22% decrease. Instead, the exothermic heat-source term that appears directly in the energy equation is scaled by Γ which is increased from 0.1 to 0.4 almost doubling the value of $Re_z^{-1/2}Nu_z$ from 0.5766 to 0.8956. Because the effects of Γ on $Re_z^{-1/2}Sh_z$ are indirect, mediated only by the coupled temperature field, no concentration profile is provided here, and the effect of Γ is correspondingly small, decreasing from 0.6156 to 0.6123.

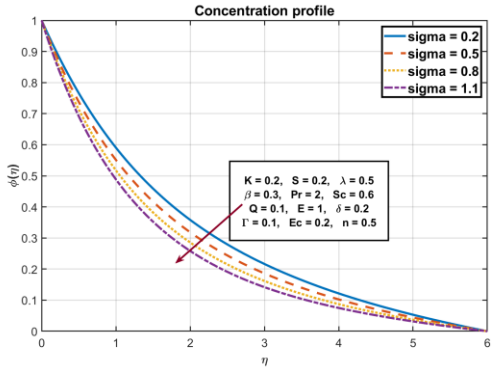
5.5 Schmidt Number (Sc), Reaction-Rate (σ), and Fitted-Rate Exponent (n)



(a) $\phi(\eta)$ vs. Sc

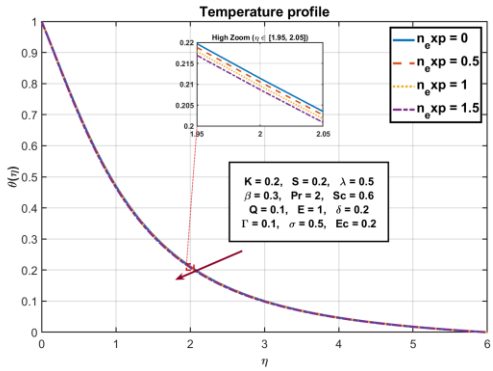


(b) $\theta(\eta)$ vs. σ

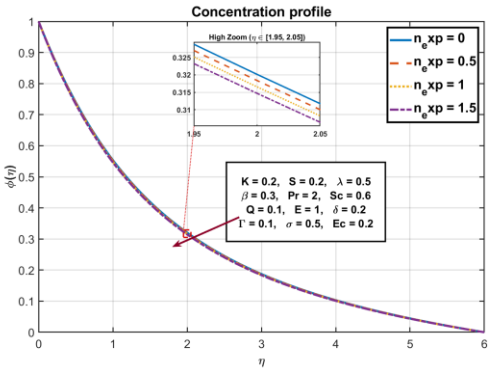


(c) $\phi(\eta)$ vs. σ

Figure 8: $\phi(\eta)$ vs. Sc



(a) $\theta(\eta)$ vs. n



(b) $\phi(\eta)$ vs. n

Figure 9: $\theta(\eta)$ vs. n

The Sherwood number is the parameter in this study that has the greatest effect on Sc. As Sc changes between 0.2 and 1.4 (with $Re_z^{-1/2}Sh_z$ increasing from 0.4291 to 0.9291), a larger Sc leads to a thin concentration boundary layer and to an increase in $Re_z^{-1/2}Sh_z$ by more than doubling. The same range of $Re_z^{-1/2}Nu_z$ also sees a slight decrease from 0.6022 to 0.5445 due to only weak feedback from ϕ to the energy equation. The reaction-rate parameter σ acts similarly: as it rises from 0.2 to 1.1, more species is consumed, lifting $Re_z^{-1/2}Sh_z$ from 0.5344 to 0.7543 while $Re_z^{-1/2}Nu_z$ eases only slightly, from 0.5850 to 0.5638. The

change in n in the exponent in the fitted rate is the smallest of the three, increasing the sensitivity of the reaction rate to temperature by 0.5% when n is stepped from 0 to 1.5 which raises $Re_z^{-1/2}Nu_z$ from 0.5720 to 0.5866 and $Re_z^{-1/2}Sh_z$ from 0.6089 to 0.6303.

6 Conclusion

This paper aimed to model and numerically solve the unsteady Jeffrey-fluid flow, heat transfer and mass transfer in the presence of a temperature dependent (Arrhenius) reaction in the concentration equation along a stretching cylinder. After reducing the conservation laws to a similarity ODE system and solving the 8th order BVP using `bvp4c` several things have been observed:

- The momentum equation is independent of the temperature and concentration, thus only four out of thirteen parameters will influence the velocity field, namely K, S, β and λ.
- The velocity and temperature fields become better with increasing curvature parameter and the concentration profile exhibits the crossover behaviour, such that the concentration profile around the walls increases with curvature, which results in higher heat-transfer and mass-transfer rates and higher skin-friction. Unlike the temperature and concentration profiles, the velocity field is affected in the opposite way by the Deborah number β, which increases all three gradients that define the Nusselt and Sherwood numbers, but which has the opposite effect on the velocity field; likewise, the relaxation-to-retardation time ratio λ has opposite effects on these three gradients. The value of the unsteadiness parameter S falls between the above two, thus increasing the skin friction and decreasing the heat and mass transfer.
- The single most important effect on the Nusselt number is that of Q and the single most important effect on the Sherwood number is that of Sc of all the tested variables.
- The most striking activation energy effects for mass transfer are that an increase in E decreases the reaction by almost a quarter, decreasing the Sherwood number, while increases in Γ and σ increase the Nusselt and Sherwood numbers, respectively.
- None of these limits recovers the Newtonian limit (both β and λ go to zero at the same time), it is the flat-plate limit (→0 separately) that is recovered.

The only other study that comes close to this problem involves the inclined-cylinder study by Hayat et al. [12] which considered double stratification instead of the activation energy reaction, but maintained the unsteadiness, dissipation, and heat-generation terms that are missing from that model seems, to the authors' knowledge, to be new. The practical motivation is clear: while all three of the applications listed above – wire drawing, fibre spinning and polymer extrusion – draw material off a surface which is closer to a cylinder than a flat sheet, the model that captures curvature and viscoelastic memory will offer something a flat-plate analysis cannot. The present model is rather limited, with the relaxation time, the retardation time, a first order homogeneous reaction; extending it to other types of constitutive models, to nonlinear radiation, to magnetic fields, to other curved geometries, or to an experimental test of the Deborah-number/activation-energy coupling on mass transfer would all be natural next steps.

References

[1] B. C. Sakiadis, "Boundary-layer behavior on continuous solid surfaces: II. The boundary layer on a continuous flat surface," *AIChE Journal*, vol. 7, no. 2, pp. 221–225, 1961.

[2] L. J. Crane, "Flow past a stretching plate," *Zeitschrift für Angewandte Mathematik und Physik*, vol. 21, no. 4, pp. 645–647, 1970.

[3] L. J. Grubka and K. M. Bobba, "Heat transfer characteristics of a continuous, stretching surface with variable temperature," *Journal of Heat Transfer*, vol. 107, no. 1, pp. 248–250, 1985.

[4] M. E. Ali, "Heat transfer characteristics of a continuous stretching surface," *Wärme- und Stoffübertragung*, vol. 29, no. 4, pp. 227–234, 1994.

[5] C. Y. Wang, "Fluid flow due to a stretching cylinder," *Physics of Fluids*, vol. 31, no. 3, pp. 466–468, 1988.

[6] A. Ishak and R. Nazar, "Laminar boundary layer flow along a stretching cylinder," *European Journal of Scientific Research*, vol. 36, no. 1, pp. 22–29, 2009.

[7] A. Ishak, R. Nazar, and I. Pop, "Unsteady mixed convection boundary layer flow due to a stretching vertical surface," *Arabian Journal for Science and Engineering*, vol. 31, no. 2, 2006.

[8] T. Hayat, Z. Iqbal, M. Mustafa, and A. Alsaedi, "Unsteady flow and heat transfer of Jeffrey fluid over a stretching sheet," *Thermal Science*, vol. 18, no. 4, pp. 1069–1078, 2014.

[9] T. Hayat, S. Asad, A. Alsaedi, and F. E. Alsaadi, "Radiative flow of Jeffrey fluid through a convectively heated stretching cylinder," *Journal of Mechanics*, vol. 31, no. 1, pp. 69–78, 2015.

[10] M. Imtiaz, T. Hayat, and A. Alsaedi, "MHD convective flow of Jeffrey fluid due to a curved stretching surface with homogeneous–heterogeneous reactions," *PLOS ONE*, vol. 11, no. 9, Art. no. e0161641, 2016.

[11] K. U. Rehman, A. A. Khan, M. Y. Malik, and O. D. Makinde, "Thermophysical aspects of stagnation point magneto-nanofluid flow yields by an inclined stretching cylindrical surface: A non-Newtonian fluid model," *Journal of the Brazilian Society of Mechanical Sciences and Engineering*, vol. 39, pp. 3669–3682, 2017.

[12] T. Hayat, S. Qayyum, M. Farooq, A. Alsaedi, and M. Ayub, "Mixed convection flow of Jeffrey fluid along an inclined stretching cylinder with double stratification effect," *Thermal Science*, vol. 21, no. 2, pp. 849–862, 2017.

[13] D. J. Samuel, K. S. Adegbie, and A. J. Omowaye, "Significance of non-uniform heat generation and convective boundary conditions in heat and mass transfer flow of Jeffrey fluid in the presence of Arrhenius activation energy and binary reaction," *The European Physical Journal Special Topics*, vol. 232, no. 6, pp. 877–891, 2023.

[14] M. Jawad, A. B. M. Ali, W. Abdelfattah, and G. Bognár, "Numerical modelling of heat transfer and flow efficiency in the stretching process and extrusion of Jeffrey fluid in a heated cylinder," *International Journal of Thermofluids*, vol. 29, Art. no. 101395, 2025.

[15] M. Jawad, A. B. M. Ali, A. Majeed, N. S. S. Singh, A. K. A. Jawwad, H. A. Garalleh, and I. Mahariq, "Significance of Cattaneo–Christov heat flux and bioconvection in magnetized Jeffrey nanofluid inside an extendable cylinder: Advances in cooling system," *Results in Engineering*, vol. 30, Art. no. 110094, 2026.

[16] J. Kierzenka and L. F. Shampine, "A BVP solver based on residual control and the MATLAB PSE," *ACM Transactions on Mathematical Software*, vol. 27, no. 3, pp. 299–316, 2001.

[17] T.-G. Fang, J. Zhang, Y.-F. Zhong, and H. Tao, "Unsteady viscous flow over an expanding stretching cylinder," *Chinese Physics Letters*, vol. 28, no. 12, Art. no. 124707, 2011.

[18] C. Y. Wang, "Free convection on a vertical stretching surface," *ZAMM—Journal of Applied Mathematics and Mechanics*, vol. 69, no. 11, pp. 418–420, 1989.